000144

BOL	FIRST Bolometer	Doc No: RAL/N0021.01
	Title: Stray light analysis, PHOT.	Date: 20-11-97
	Prepared by: M Caldwell, A Richards, B Swinyard	

CIRCULATION:

Martin Caldwell	RAL
Peter Gray	RAL
Tony Richards	RAL
Bruce Swinyard	RAL
Matt Griffin	QMW
Eli Atad	ROE
Fraser Morrison	ROE
Walter Gear	ROE

CONTENTS.

Summary.
This note is to give a description of the design features of PHOT used for stray-light control, and of the models used in the design and the prediction of the stray light performance.

It is also to describe a baseline as regards the understanding of the telescope stray light design, so that specific questions on open issues can be raised (section 3).

The design as currently defined in stray light analysis software is listed in the appendices, for independent assessment of the design.

The stray-light effects are classed into 2 types; inside-of-field (IOF) & out-of-field (OOF), and a separate analysis of the system is made for each:

- The IOF analysis concerns optical components & their immediate surrounds, contributing radiometric background due to their finite sizes. The major

contributions to this are given in section 2.1.1, table 1, and the total is < 0.15 times the telescope background. The analysis is used to propose sizes for each of the optical components & the system pupil, and the proposed sizes would reduce the aperture from F/5 to F/6 (approx. 30% loss of throughput).

- The OOF analysis concerns extended sources at wide angles from the optical beam, i.e. thermal enclosure walls & baffles, and it is to be used in radiometric design of these structures.

1. Description of stray-light design.

The PHOT-BOL optical design, and the telescope design on which it is based, is given in Ref.1.

The level of background power seen by the photometer detectors is, in the absence of stray light in BOL, limited by the on-board emission from the telescope mirrors, as these are hot (80K) relative to the instrument (15K).

The dominant source of stray light in this type of instrument *is on-board thermal emission*, reaching the detector either *directly* if emitted from components inside of the field of view (IOF), or *indirectly* if emitted e.g. by baffles outside of the field of view (OOF).

A hierarchy of the stray light terms & models is given in fig.0.

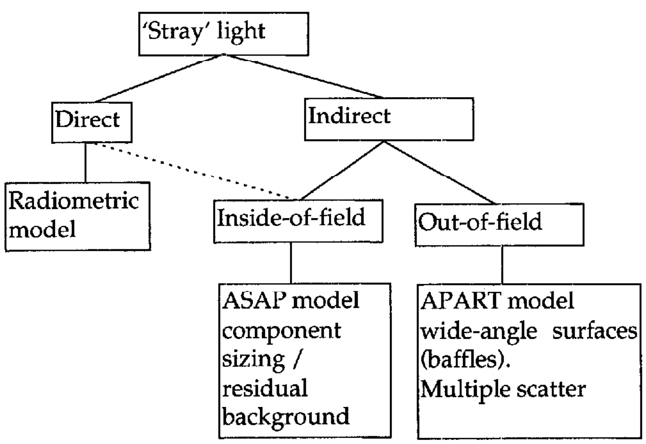

Fig.0. Stray light model hierarchy.

The FIRST telescope design is included in the ray-trace model, and assumptions about its baffling are given in section 3. The PHOT optics instrument design is shown in fig.1 in relation to the telescope and on a larger scale in fig.2.

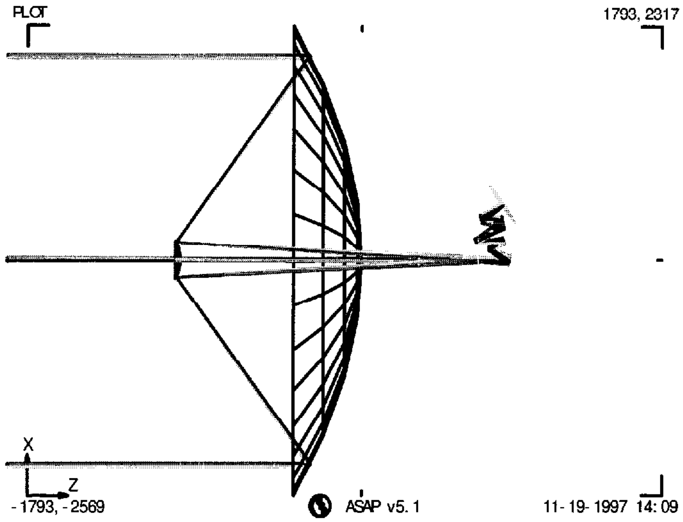

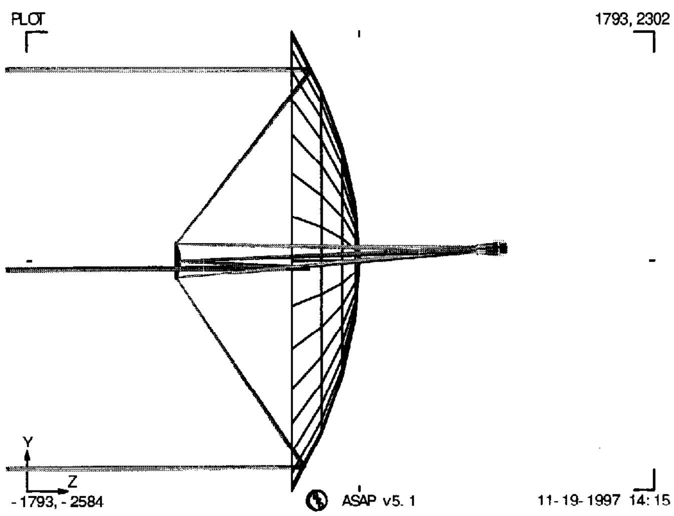

Figure.1 Ray trace of PHOT-BOL design, showing relation to FIRST telescope. Upper: side view Lower: plan view.

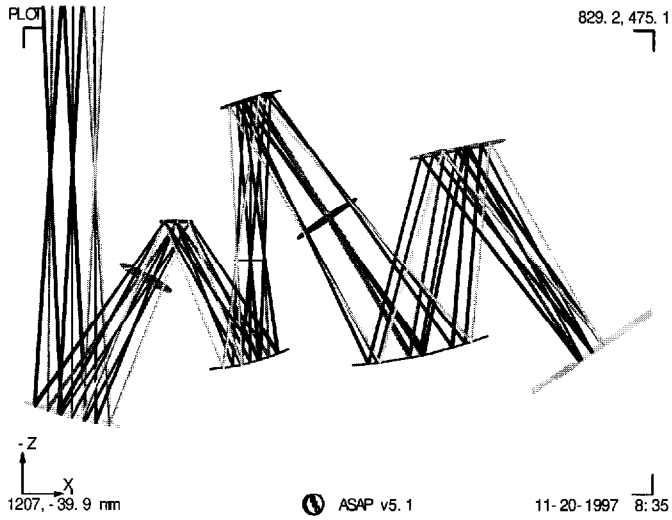
PLOT
829.2, 475.1
-Z
X
1207, -39.9 mm
ASAP v5.1
11-20-1997 8:35

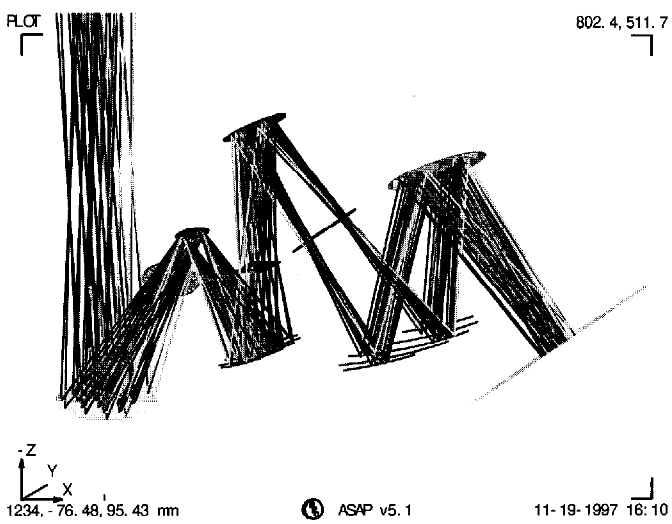
PLOT
802.4, 511.7
-Z
Y
X
1234, -76.48, 95.43 mm
ASAP v5.1
11-19-1997 16:10

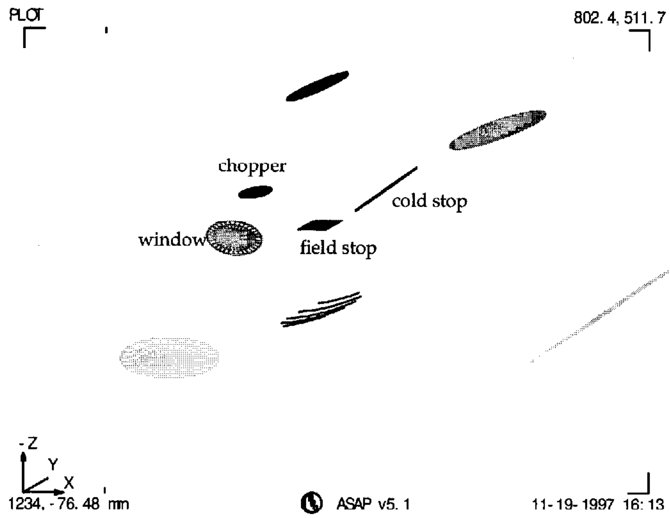

Figure.2 Ray trace of PHOT-BOL design, side view & oblique views with & without rays.

The instrument thermal configuration is shown in more detail in fig.3, where it can be seen that the optical path passes via several thermal enclosures of ever decreasing temperature.

Figure.3 PHOT-BOL optical & thermal enclosure layout.

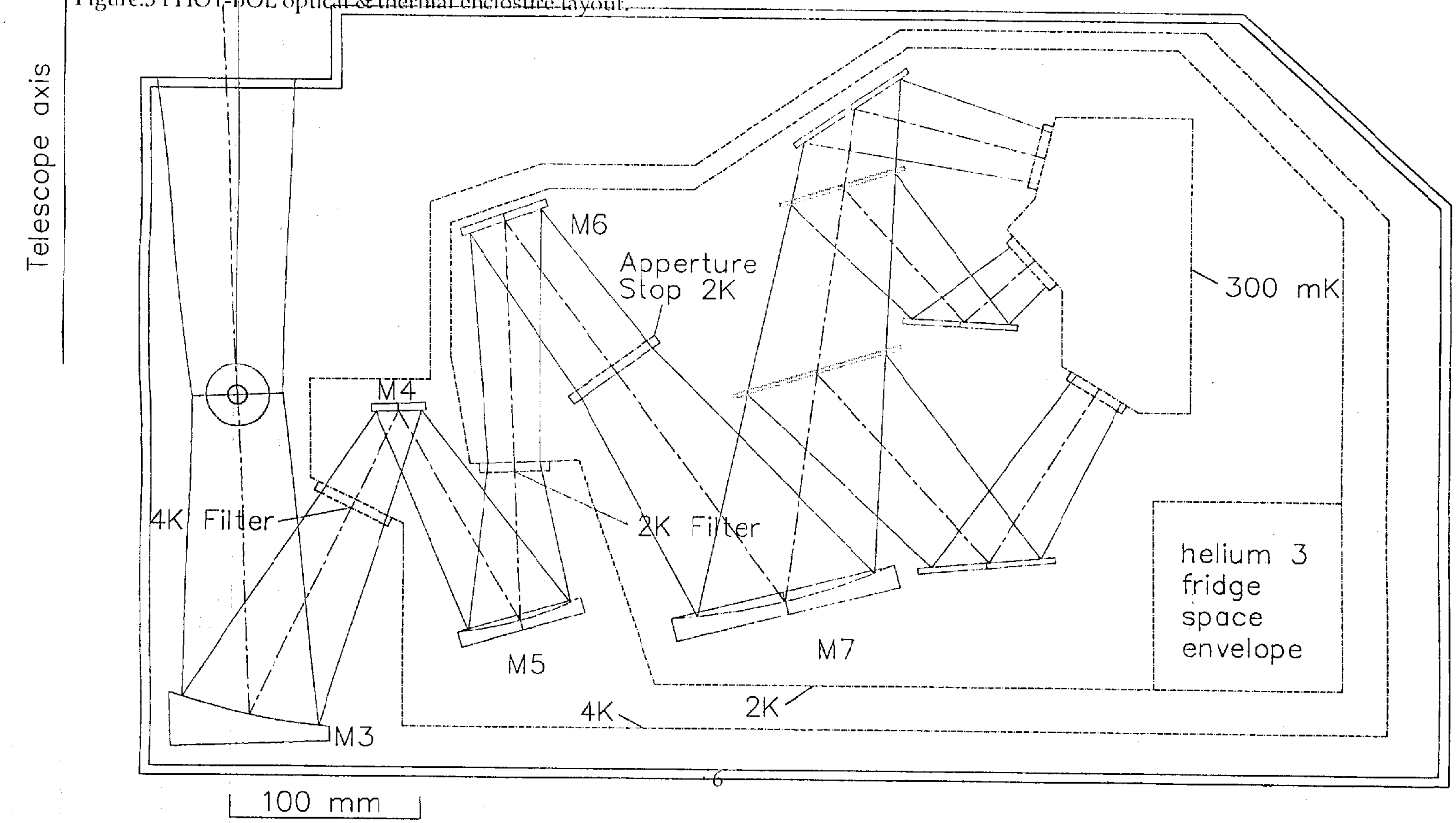

1.1 Direct stray light.
The detector sees directly some thermal emission from all of the mirrors & filters in the optical path. The contribution of these is calculated in ref.2 & 3. Since the component emissivities are all low (assumed ε=0.01), their direct contributions are also low, except for the telescope mirrors as these are relatively very hot.

The design concept is that the non-optical (& high emissivity) surfaces seen by the detector are restricted to the walls within the 2K box. To achieve this the Cold Stop at the entrance of the box must realise the instrument System Aperture Stop (SAS), and the detector area must realise the System Field Stop (SFS).

By definition, all other stops in the system are *oversized* with respect to their images at the SAS & SFS, so that their edges are never seen directly by any detector. In addition the stops are configured where possible as transmissive rather than reflective, so that it is their colder side (that facing away from the incoming radiance) which is seen. As shown in fig.2 a field stop is also placed at the image plane ahead of the CS, forming the entrance to the 4K box. A pupil plane occurs at the chopper M4 , and a non-pupil plane transmissive stop is placed ahead of this, and another one ahead of M3 at the entrance of the 15K box.

The oversizing of each stop with respect to its conjugate subsequent stop includes a margin to account for geometric aberrations in the imaging between stops. The required size of this aberration margin is independent of channel wavelength. A margin for the indirect viewing of the stop edges via diffraction is also necessary, as detailed in section 2.1. This margin tends to increase in direct proportion to the wavelength. Finally a margin for mechanical tolerances of alignment must also be included. It is found that the diffraction margin required for the outermost detectors & the longest wavelengths is not practical, and so some 'leakage' of the stops is accepted for these cases (section 2.1).

1.2 Indirect stray light.

The radiance reaching the detector indirectly can come from many different paths. With the above design features to limit the direct stray light, the main indirect paths which are important are:

- Coherent scattering i.e. diffraction at edges (stops and mirrors)
- Incoherent scattering at edges and at surfaces.

These paths may involve multiple scattering events, with the radiance being heavily attenuated with each scatter event, but with the residual level at the detector being nevertheless significant because the radiance originated in a relatively hot (bright) or geometrically large region of the system.

At the BOL wavelengths the dominant scatter problem is that of diffraction. The incoherent scatter at optical surfaces is relatively small at these wavelengths, whilst the scatter at diffuse baffle surfaces can be significant since these surfaces are not perfectly black (section 2.2) ?

The best defence against indirect stray light is to limit the angular range of the OOF radiance incident on each scattering component, to the minimum level at the earliest opportunity, and this is partly achieved with the system of nested cold boxes surrounding the stops as described in section 1.2. In addition the mirror zig-zag folding is designed such that baffle tubes can be accommodated over a sufficient length of the optical path to prohibit the passage of beams directly from the 15K box to the 2K box. (i.e. along OOF paths at large off-axis angles which by-pass some mirrors).

As for the stops at pupil or image planes, the mirrors and the baffles are oversized with respect to the detector geometric beam to minimise their edge-diffraction contribution. This is important because these components are at arbitrary points in the optical path, and usually do not have colder conjugate stops farther down the system at which their diffraction may be blocked. The IOF stray light model of section 2.1 is used to determine these oversize requirements. In components where oversize to the beam's -20dB edge taper is not possible, the resulting contribution to stray light is calculated.

2. The stray light model.

In optical systems for the thermal IR (e.g. wavelength 4 to 30μm) , edge-diffraction is often described by geometric ray-tracing, of the so-called boundary-wave model of diffraction (Ref.4). At each edge where the specular beam is clipped, 'diffracted rays' are generated. These rays may be further diffracted at a subsequent aperture, to produce 'doubly diffracted rays', and so on.

This type of analysis has the following limitations:

- It doesn't allow a non-lambertian detector response to be described.
- It doesn't allow beam patterns at each component to be inspected.
- For radiance transfer calculations it uses diffractive scatter equations which are valid only at positions which are well within the geometric shadow (i.e. more than one airy disc radius from its edge). This means the model deals specifically with *indirect* stray light, and it restricts the validity to so-called 'well-baffled' systems, which cannot be achieved at longer wavelengths.

In mm-wave systems diffraction is described by the 'antenna pattern', which is the detector FOV response function, mapped onto the sky by propagating it outwards through the system (Ref.5). At the same time the beam pattern can be found at each component, and used to size the component (ideally) to be large enough that its edge-diffraction is negligible. Where significant clipping of the specular beam does occur, it has to be included as a re-definition of the beam, before onward propagation. In this model there is no distinction between *direct* and *indirect* light; the beam pattern covers both regimes as it theoretically extends from the specular beam out to very wide far-field angles.

Our instrument operates in a wavelength region in between the thermal-IR & mm-wave regions, and both types of diffraction model are employed, because.

1. The beam propagation description is needed because the system cannot be 'well-baffled', and the component sizing must be analysed in detail.
2. The beam pattern at large off-axis positions is also needed, since there are surfaces well outside the geometric beam which can nevertheless contribute strongly to stray light because they are relatively hot. To compute this data, the beam propagation method is numerically very inefficient as compared to the diffracted-ray model (the latter is efficient because it specifically traces only the stray-light rays). Also, the diffracted ray model can incorporate multiple scatter, e.g. paths including diffuse plus diffractive scatter, occurring due to limited blackness of the baffle coatings.

Here for nomenclature we refer to the beam propagation model as IOF and the diffracted-ray model as OOF diffraction. The models are implemented in the software packages ASAP© and APART respectively (both from the same corporation, ref.6).

The IOF model (section 2.1) is derived from the instrument optical design ray-trace prescription, using an automatic translator, and it includes all optical components and stops. The OOF model (section 2.2), has to additionally include the OOF baffles and other structure TBD, and so is currently not defined in detail. However the contributions from certain hot surfaces have been estimated with a certain assumed baffle geometry (section 3.2 & Ref.3).

2.1 Inside-of-field (ASAP).

2.1.1 Beam propagation model & IOF backgrounds.

The ASAP model geometry is that shown in fig.2, and a text listing is given in the appendix. The current model has components as either circular or rectangular, but since the system has a circular pupil & a square field, the optimum shape of some components (between image & pupil planes) will actually be a 'race-track', to save mass.

To calculate the IOF stray radiance from the component surrounds, the detector beam is propagated outwards through the system, and its beam pattern is computed at each component in turn. The proportion of the beam flux which 'misses' the component, i.e. lies on its surround is then found, and combined with the assumed ε and T values to give the background contribution (see table 1). For non-pupil-plane components this 'clipping' of the beam by the component edge is worst for the outermost detector of the array, in some particular direction. The effect is also worst for the longest wavelength array, and the wavelength assumed is 0.5mm, close to the centre wavelength of band 3.

For onward propagation from the component, the beam as clipped by that component should be propagated, since the clipping does affect the downstream beam pattern, and may lead to further clipping which would not otherwise occur (this is equivalent to multiple diffraction in the ray-model). Therefore in the present model, when the clipping is significant, the beam is re-defined to include it.

The details of the computation and the format of the beam patterns is given in Ref.7, which is to be updated for new design. Here we give examples to summarise the important components.

Beginning at the **detector**, this is a bare bolometer (no cone) and is modelled as a point detector with Lambertian response. The clipping of this pattern by the last two mirrors of the system (and the beamsplitters) is not modelled. The first component where clipping is applied is the **cold stop**, the exit to this box. At this point the surround is taken to be the full hemisphere. In this way the background of the whole cold box is included without reference to which part of the box it comes from. The beam pattern at the cold stop is shown in fig.4.

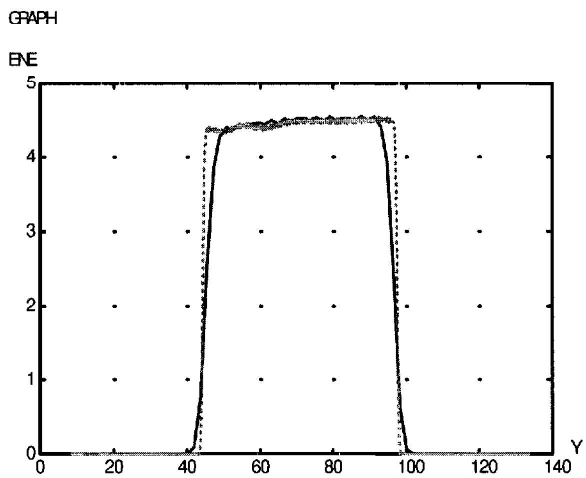

Fig.4 Beam pattern cross-section (flux versus position in mm) at **cold stop**.
Dotted line: geometric beam (short wavelength). Solid line=BOL beam.

Here the dotted line is a computation at short-wavelength, to show the geometric beam, and the solid line is that at the BOL wavelength. The pattern has a top-hat shape as expected due to the clipping of a lambertian source. The beam edges are blurred at the longer wavelength. This is because the pattern is defined only up to the spatial resolution which corresponds to the angular acceptance of the subsequent system, and this resolution is approx. equal to the wavelength (0.5mm in this case). The reason for this is that definition of the long-wavelength beam to higher resolution leads to a very lengthy computation which is also inefficient, since the larger diffraction angles corresponding to the higher resolution are in any case blocked at the next field stop. Strictly speaking this means that the beam patterns computed at a subsequent component is only accurate if that component lies behind a field stop. This is thought not to be problematic in our case since for the components between the cold stop and the field stop, the beam pattern is not needed to a high degree of accuracy because the components can all be oversized with margin added.

All of the **mirrors between the cold stop & field stop** are in far-field regions, and it is found that in order to limit clipping to the $< 1\%$ flux level (in mm-wave terms, -20dB edge taper), and oversize of approx. 20 % in radius is sufficient.

At the **field stop**, the oversize required with respect to the detector array is by an amount of at least Fλ in semi-diameter (this stop is rectangular) , where F is the f-number at this position. For the long-wavelength channel with 16 detectors spaced on a 0.5Fλ pitch, the resulting oversize is 20%.

The next components are **M5, M4 & the window**. These are given the nominal 20 % oversize for <1% clipping, except for the chopper. This is a special case; because it is at a pupil plane the diffraction from the cold stop is re-focused here. The question of relative sizing of the three pupil-plane stops (M2, M4 & cold stop) is dealt with in the next section.

The next component is **M3**. This is in a near-field region, being close to the telescope image plane, and the oversize allowed is limited by its close proximity to the box wall. This means that clipping does occur here, and is shown by the beam pattern in fig.5. This is for the worst-case field position which is the -X extreme (co-ordinate system as per fig.1). The effect of this clipping on the subsequent propagation is not included as the current model can only handle clipping which occurs in far-field parts of the beam.

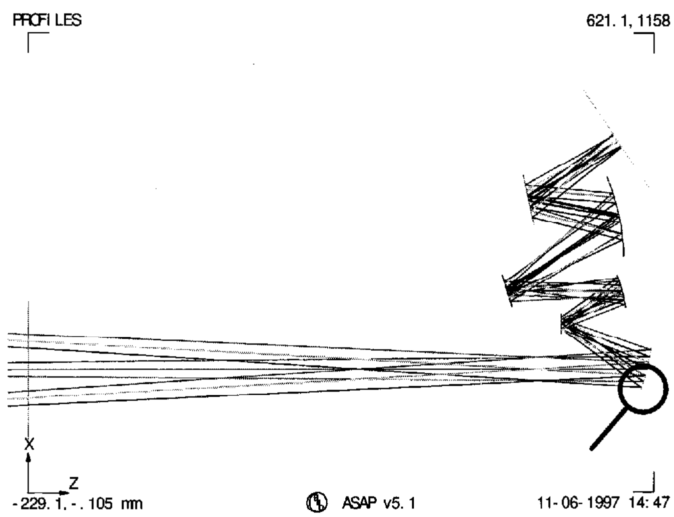

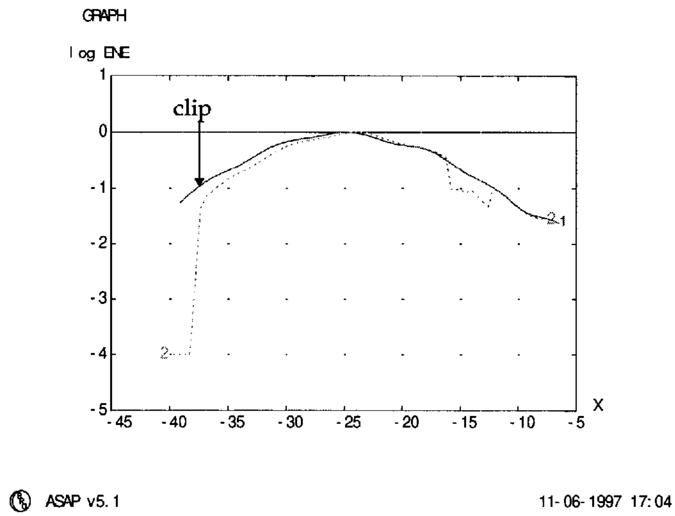

Fig.5. Clipping at M3. Upper plot shows location of clip. Lower plot is beam pattern (flux vs mm, log scale), solid line=no clipping, dotted line=with clipping.

The next component is the **M1 rear-side**. Here the worst case detector is the +Y field position, and the beam pattern in the Y-direction is shown in figure.6. Here oversizing of the M1 cut-out is not allowable, as it would increase the obscuration factor of the telescope. As shown in the figure, the clipping is at a relatively low level (log scale), and so its effect on subsequent propagation is not included.

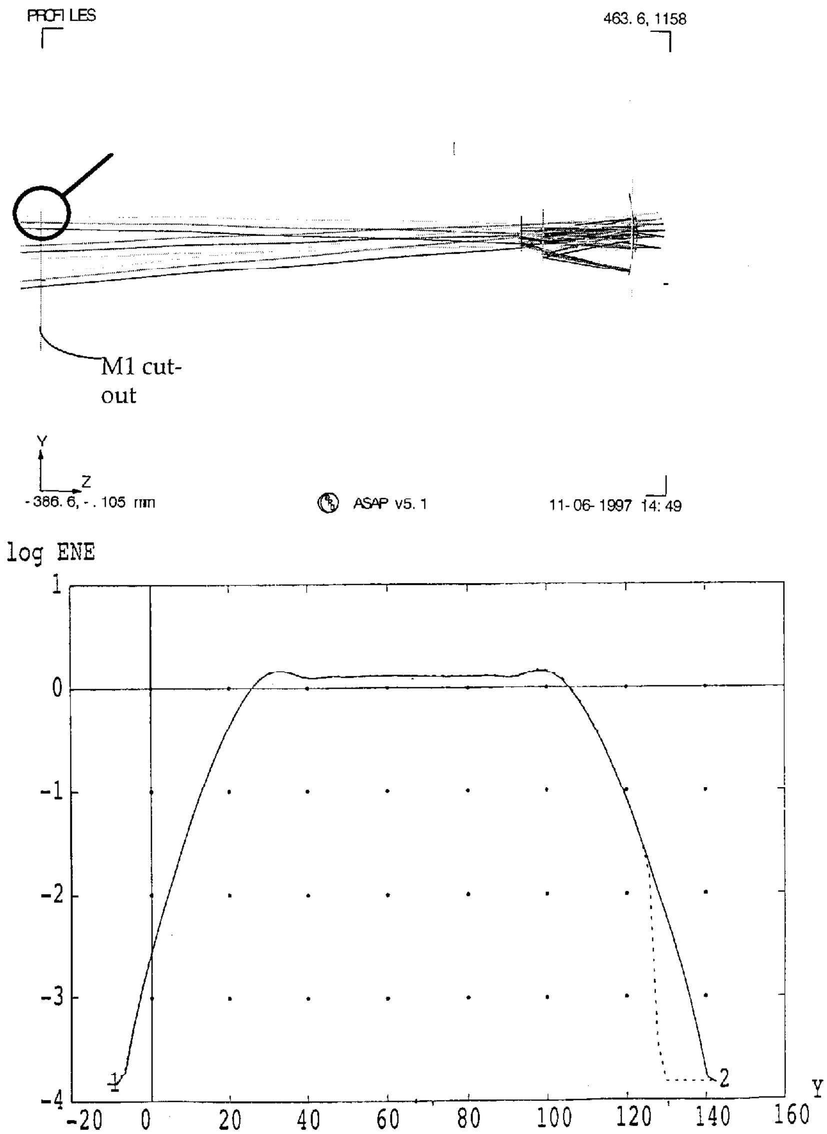

Fig.6 Clipping at M1 cutout. Upper plot shows location of clip. Lower plot is beam pattern (flux vs mm, log scale), solid line=no clipping, dotted line=with clipping.

The pattern at **M2** is shown in fig.7, at both short wavelength (geometric beam) & long wavelength, as for the cold stop. The case shown is the outer detector as per fig.6, and since this beam is not perpendicular to the plane of M2, the flux pattern has a sloping top. In this plot the portion of the long wavelength beam which lies outside of the geometric beam, is that which lies on the M2 surround.

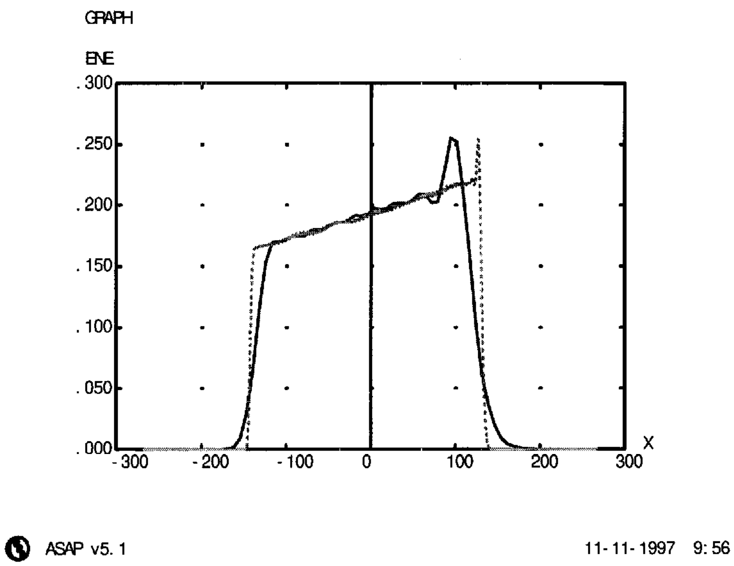

Fig.7 flux versus position in mm at **M2**.
Dotted line: geometric beam (short wavelength). Solid line=BOL beam.

The beam is next propagated onto **M1**, for which it is assumed there is no surrounding structure on the outer edge (section 3). At this point there is clipping of the centre portion of the beam by the M1 cutout, but this central obscuration is not yet included in the propagation model. (The 'surround' seen by the portion passing through M1 cutout is assumed to be a view back to the instrument box at 15k, and this is not included as it is relatively cold).

The beam is finally propagated from M1 onto the **sky** at this point the beam is clipped by the spider structure and by the edge of M2. These features have not yet been included in the propagation model. The pattern on the sky (flux versus off-axis angle) is the instrument FOV response function. In the absence of clipping this is equivalent to the imaging point spread function for a 3.5m circular aperture, nominal image aberration effects of the system.

The beam patterns at all components are given in ref.7.

From the above model the calculated IOF background contributions are as given in table 1. For each component figures are given for both the centre detector and the particular outer detector having worst-case clipping. The cold stop and M2 are at pupil planes and so their levels will be similar for the centre & the outer detectors. For M2 the calculation includes the effect of pupil aberration, and it is expected that the background will be somewhat lower at the centre detector where the aberration is smaller. Therefore a '<' symbol is included in this entry.

It can be seen that the largest contributors are the M1 rearside & the M2 surround, as these are the hottest viewed objects, although their contribution is still an order of magnitude less than the direct contribution of the telescope.

Component	**fraction of flux lost**		**Surround emissivity**	**Temp**	**Fractional background, band 3**	
	centre det.	**outer det.**			**centre det.**	**outer det.**
Cold stop	128 lamb'n	128 lamb'n	1.0	2	0.0026	0.0026
M3 surround	0	0.04	0.15	15	~ 0	4e-4
rear-side of M1	0	0.0145	0.15	80	~ 0	0.11
M2 surround	<0.02	0.02	0.15	80	<0.15	0.15

Table 1. Background levels due to beam clipping, as fractions of telescope background as per ref.3.

2.1.2 Proposed pupil sizing.

The above IOF background levels arise due to restrictions on component sizes, and the only way to reduce them is to undersize the instrument pupil of FOV with respect to the telescope, e.g. to stop the PHOT beam down from its F/5 relative aperture, trading-off some throughput for improved stray-light rejection.

In this regard the clipping at M3 is not problematic, as it produces a negligible level, even at the outer detector.

For the M1 cutout and M2, it can be seen from e.g. figure 7, that a significant undersize of the BOL beam (approx. 15% in radius) would be necessary in order to completely remove the diffraction 'overspill' on the M2 surround. Such an undersize is thought to be an unreasonable amount for the throughput/background trade-off, losing approx. 30% in throughput, in order to remove only <15% of the background level, and this applying only to the longest wavelength channel. It is therefore proposed that the background levels of table 1 be accepted, and no diffraction-undersize be applied to PHOT.

There is also the matter of aberration undersize and alignment margin to consider. Here the aberration is the variation of pupil position with field angle (detector position in the array), and this is not shown in the above plots as these are for single detectors only.

This undersize is more important than that for diffraction, because it applies to all wavelengths in the PHOT bands, and to out-of-band stray light at all wavelengths (it is a purely geometric effect). The proposed undersizes are detailed in table 2.

Component	Geometric beam radius in mm	Undersize wrt previous pupil		
		Aberration	alignment margin, mm	net stop radius, mm
Chopper M4	10.7	1.6	0.1	0.9
Cold stop	27.8	0	0.1	23.3

Table 2. Pupil stop undersizes.

Here the aberration undersize is allocated to M4 to prevent viewing of M2 surround. At the cold stop no additional aberration undersize is used, since the viewing of the M4 surround is less problematic (this being at 4K).

The resulting net radius for the cold stop aperture leads to a reduction in PHOT relative aperture from the design F/5 to approx. F/6. Alternatively if we need to maintain the F-number at F/5, the PHOT magnification (focal length) could be changed. In either case the throughput reduction is by a factor of $(5/6)^2$ = 70 %. To improve this parameter the design could be re-optimised to reduce the pupil aberration & to take into account the new F-number.

2.2. Out-of-field (APART).
To date this contribution has been estimated for the case of structure seen by M3 (ref.3, section 7), while the detailed APART model & baffle design is TBD upon finalising the optics design.

3. Areas of uncertainty & questions.
The items which have uncertain properties , and their assumed parameters are:

3.1. IOF model.
Following the beam along its path, the assumptions are:

Telescope M1 surround: there is *no* structure.
Telescope M2 surround: there is a conical baffle, with emissivity ~ 1, at 80 K.
Telescope M1 rear-side, surrounding central cut-out: Surface has ε~ 0.15, T=80K
BOL M3 surround: The wall is at 12mm from M3 centre, with ε~ 1, T=15K.
BOL wall near HET: There is no cut-out as yet, since dimensions are TBD.

The assumed aperture sizes for these components are included in the ASAP listing (Appendix 1).

3.2 OOF model.

Telescope spider structure: ε~ 0.01, T=80K.

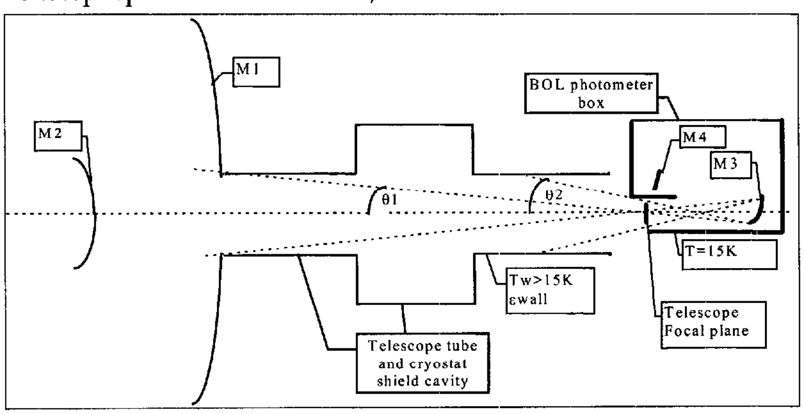

Structure between Telescope & BOL. As per Ref. 3, fig. 2 (reproduced below), assumed ε~ 0.15, T=80K.

4. References.

Ref.1 Optical Design, 7-11-97. E. Atad (see also BOL/QMW/M/0024.10).
Ref.2 PHOT-BOL radiometric model. M Griffin
Ref.3 "Level of photometer background signal from the optics" BOL/RAL/N0007.1. A Richards.
Ref.4 "Method for calculating diffraction effects in opto-mechanical systems of arbitrary geometry" A Greynolds. Proc. SPIE. Vol.257, pp.64-77 (1980).
Ref.5 "Quasi-optical antennas for radiometric remote-sensing" R J Martin & D H Martin. IEE. Electronics & Communication Engineering Journal. (Feb. 1996).
Ref.6. Advanced systems analysis program (ASAP). Publ. Breault Research Org. Inc. 6400 East Grant Road, Tuscon, AZ, USA.
Ref.7 "Beam patterns in PHOT-BOL design & telescope". BOL/RAL/N006.4 M. Caldwell.

Appendix 1. PHOT Optical prescription.

(CODEV ray-trace).

```
RDM;LEN     "VERSION: 8.20 A     LENS VERSION: 45     Creation Date: 7-Nov-1997"
TITLE ' BOL PHOT with new array of detectors 7/11/97'
EPD  3283.41
DIM  M
WL   200000.0
REF  1
WTW  1
INI  ''
XAN  0.0367 0.0367 0.0367 0.0 0.0 0.0 -0.0367 -0.0367 -0.0367
YAN  0.1462 0.1829 0.2196 0.1462 0.1829 0.2196 0.1462 0.1829 0.2196
VUX  0.0169941875 0.0 0.0 0.0 0.0 0.0 0.0 0.0 0.0
VLX  0.0169941875 0.0 0.0 0.0 0.0 0.0 0.0 0.0 0.0
VUY  0.016993876832 0.0 0.0 0.0 0.0 0.0 0.0 0.0 0.0
VLY  0.016993876832 0.0 0.0 0.0 0.0 0.0 0.0 0.0 0.0
PRV
 PWL 5000.0 4000.0 3000.0 2000.0 1000.0
 'BAF2R' 1.451 1.4567 1.4616 1.4646 1.4686
 'CAF2R' 1.3996 1.4096 1.4179 1.4239 1.4289
 'BAF2' 1.4547 1.4604 1.4653 1.4683 1.4723
 'CAF2' 1.40213 1.41213 1.42043 1.42643 1.43143
 'ZNSE' 2.41582 2.4195 2.4232 2.4276 2.4792
 'ZNSER' 2.42582 2.4295 2.4332 2.4376 2.4892
END
SO   0.0 0.1e11
S    -3046.246 -1396.3648 REFL
```

```
 CON
 K -1.0
S  -267.82995 0.0 REFL
 STO
 CON
 K -1.2387718
 DAR
S  0.0 0.0
 ADE 2.19762; BDE 0.0; CDE 0.0
S  0.0 1398.110199
S  0.0 975.0
S  0.0 170.0
S  0.0 0.0
S  -340.0 -180.0 REFL
 BEN
 ADE 0.0; BDE 14.0; CDE 0.0
S  0.0 128.83 REFL
 BEN
 ADE 0.0; BDE -28.0; CDE 0.0
S  -176.4174 -84.4666 REFL
 XTO
 CUX -0.00510939469512
 K 0.0; IC Yes
 A 0.0; B 0.0; C 0.0; D 0.0
 BEN
 ADE 0.0; BDE 14.0; CDE 0.0
S  0.0 -129.18322
S  0.0 100.34 REFL
 CCY 0
 BEN
 ADE 0.0; BDE -17.0; CDE 0.0
S  0.0 150.0
S  -347.12645 -170.0 REFL
 CCY 0
 XTO
 CUX -0.0024768494762; CCX 0
 K 0.0; IC Yes
 A 0.0; B 0.0; C 0.0; D 0.0
 BEN
 ADE 0.0; BDE 22.0; CDE 0.0
S  0.0 198.0 REFL
 BEN
 ADE 0.0; BDE -22.0; CDE 0.0
SI 0.0 0.0 AIR
```

```
GO

********************CODEV to ASAP conversion*********************
* BOL PHOT with new array of detectors 7/11/97
* systems units are in millimeters
*****************************************************************
*****************************************************************
* Technical notes:                                    *
* CODEV writes out certain data in lower case letters. Since these  *
* may be incompatible with ASAP, edit these to upper case letters.  *
*                                                     *
* This procedure uses the CODEV reference rays to determine aperture*
* dimensions. In certain situations (e.g., near image planes), it   *
* may be necessary to reset the dimensions of the LOCAL box manually*
* to avoid ray clipping.                              *
*****************************************************************
SYSTEM NEW
UNITS MM
OSIZ=0.2
SURFACE
 OPTICAL Z 0  -3046.246000    -1.000000
 LOCAL -1707.946 1707.946 -1707.946 1707.946 -574.559 574.559 Z
 LOCAL EXPAND .05
 OBJECT;.1 *MIRROR  1
 INTERFACE 1
 SHIFT Z  0.000000
SURFACE
 OPTICAL Z 0  -267.829950    -1.238772
 LOCAL -137.299 137.299 -137.299 137.299 -41.588 41.588 Z
 LOCAL EXPAND .05
 OBJECT;.1 *MIRROR  2 STOP
 INTERFACE 1
 SHIFT Z -1396.364800
SURFACE
 PLANE Z 0
 LOCAL  -67.639  67.639 -67.639  67.639 -0.100  0.100 Z
 LOCAL EXPAND .05
 OBJECT;.1 *OPTIC  5
 INTERFACE 0 1 AIR
 ALIGN 0 0 1 0.000000 0.038346 0.999265
 SHIFT  0.000000 53.612354  0.717103
SURFACE
 OPTICAL Z 0  -340.000000
 !LOCAL  -38.330  38.330 -38.330  38.330 -2.601  2.601 Z
```

```
 LOCAL -2@43 -41-82 -41+82 -2.601 2.601 ! mg, 2-1-97 increased size to cover
chopped FOV
 !LOCAL EXPAND .05
 OBJECT;.1 *MIRROR 8
 INTERFACE 1
 ALIGN 0 0 1 -0.241922 0.037207 0.969582
 SHIFT 0.000000 97.518869 1144.874967
SURFACE
 PLANE Z 0
 LOCAL -12.368 12.368 -12.368 12.368 -0.100 0.100 Z
 LOCAL EXPAND .05
 OBJECT;.1 *MIRROR 9
 INTERFACE 1
 ALIGN 0 0 1 -0.000000 0.038346 0.999265
 SHIFT 84.504881 91.424469 986.061292
SURFACE !***THIS SURFACE IS PROBABLY NOT CORRECT***
 !OPTICAL Z 0 -176.417400
 BICONIC Z 0 -195.7179 -176.4174
 LOCAL -27.618 27.618 -27.618 27.618 -2.610 2.610 Z
 LOCAL EXPAND OSIZ. !.05
 OBJECT;.1 *MIRROR 10
 INTERFACE 1
 ALIGN 0 0 1 0.241922 0.037207 0.969582
 SHIFT 144.986903 95.786366 1099.727769
SURFACE
 PLANE Z 0
 LOCAL -21.208 21.208 -21.208 21.208 -0.100 0.100 Z
 LOCAL EXPAND OSIZ. !.05
 OBJECT;.1 *MIRROR 12
 INTERFACE 1
 ALIGN 0 0 1 0.292372 0.036671 0.955601
 SHIFT 144.986903 87.593686 886.235086
SURFACE !***THIS SURFACE IS PROBABLY NOT CORRECT***
 ! OPTICAL Z 0 -347.126450
 BICONIC Z 0 -403.73870601 -347.12645
 LOCAL -47.347 47.347 -47.347 47.347 -3.893 3.893 Z
 LOCAL EXPAND OSIZ. !.05
 OBJECT;.1 *MIRROR 14
 INTERFACE 1
 ALIGN 0 0 1 0.207912 0.037508 0.977428
 SHIFT 284.975254 95.552126 1093.623707
SURFACE
 PLANE Z 0
 LOCAL -32.866 32.866 -32.866 32.866 -0.100 0.100 Z
 LOCAL EXPAND OSIZ. !.05
```

```
 OBJECT;.1 *MIRROR 15
 INTERFACE 1
 ALIGN 0 0 1  0.207912  0.037508  0.977428
 SHIFT 314.495444  89.132291 926.329523
SURFACE
 PLANE Z 0
 LOCAL  -55.272  55.272  -55.272  55.272  -0.100  0.100 !Z
 LOCAL EXPAND .05
 OBJECT;.1 *IMAGE  16
 INTERFACE 0 1
 ALIGN 0 0 1  0.559193  0.031791  0.828428
 SHIFT 425.215639  95.426815 1090.358232
!SEARCH SEQ FOR
RAYS Z 16778.6805; 0 -1559.620; 0 1559.620
SOURCE DIR  0.000641  0.003192  0.999995
RAYS Z 16778.6805; 0 -1559.620; 0 1559.620
SOURCE DIR -0.000641  0.003192  0.999995
RAYS Z 16778.6805; 0 -1559.620; 0 1559.620
SOURCE DIR  0.000000  0.003192  0.999995
RAYS Z 16778.6805; 0 -1559.620; 0 1559.620
SOURCE DIR  0.000000  0.003833  0.999993
RAYS Z 16778.6805; 0 -1559.620; 0 1559.620
SOURCE DIR  0.000000  0.002552  0.999997
RAYS Z 16778.6805; 0 -1559.620; 0 1559.620
SOURCE DIR  0.000641  0.002552  0.999997
RAYS Z 16778.6805; 0 -1559.620; 0 1559.620
SOURCE DIR  0.000641  0.003833  0.999992
RAYS Z 16778.6805; 0 -1559.620; 0 1559.620
SOURCE DIR -0.000641  0.002552  0.999997
RAYS Z 16778.6805; 0 -1559.620; 0 1559.620
SOURCE DIR -0.000641  0.003833  0.999992
RAYS Z 16778.6805; -1559.620 0; 1559.620 0
SOURCE DIR  0.000641  0.003192  0.999995
RAYS Z 16778.6805; -1559.620 0; 1559.620 0
SOURCE DIR -0.000641  0.003192  0.999995
RAYS Z 16778.6805; -1559.620 0; 1559.620 0
SOURCE DIR  0.000000  0.003192  0.999995
RAYS Z 16778.6805; -1559.620 0; 1559.620 0
SOURCE DIR  0.000000  0.003833  0.999993
RAYS Z 16778.6805; -1559.620 0; 1559.620 0
SOURCE DIR  0.000000  0.002552  0.999997
RAYS Z 16778.6805; -1559.620 0; 1559.620 0
SOURCE DIR  0.000641  0.002552  0.999997
RAYS Z 16778.6805; -1559.620 0; 1559.620 0
SOURCE DIR  0.000641  0.003833  0.999992
```

```
RAYS Z 16778.6805; -1559.620 0; 1559.620 0
SOURCE DIR -0.000641  0.002552  0.999997
RAYS Z 16778.6805; -1559.620 0; 1559.620 0
SOURCE DIR -0.000641  0.003833  0.999992
MOVE TO Z  -3283.410

OBJECT numbers/names:
  1=MIRROR  1
  2=MIRROR  2 STOP
  3=OPTIC   5
  4=MIRROR  8
  5=MIRROR  9
  6=MIRROR 10
  7=MIRROR 12
  8=MIRROR 14
  9=MIRROR 15
 10=IMAGE  16
 11=IDEALENS
 12=SKY
 13=COLDS
 14=FIELDS
 15=WINS
--- CON ALL
--- PRI OBJ

 OBJECT    1: MIRROR  1
 Physical Surface     1 (OPTICAL )
    Box X -1793.     1793.   Y -1793.     1793.    Z -603.3     603.3
       width= 3586.7        width= 3586.7        width= 1206.6
 Interface Reflectivity 1.000000

 OBJECT    2: MIRROR  2 STOP
 Physical Surface     2 (OPTICAL )
    Box X -144.2     144.2   Y -144.2     144.2    Z -1440.   -1353.
       width= 288.33        width= 288.33        width= 87.335
 Interface Reflectivity 1.000000

 OBJECT    3: OPTIC   5
 Physical Surface     3 (PLANE   )
    Box X -71.02     71.02   Y -17.36     124.6    Z -2.111     3.545
       width= 142.04        width= 141.95        width= 5.6566
       Transmission 1.000000 Media   0   0

 OBJECT    4: MIRROR  8
 Physical Surface     4 (OPTICAL )
```

Box X -44.37 44.37 Y -27.33 140.4 Z 1127. 1162.
width= 88.742 width= 167.76 width= 35.240
Interface Reflectivity 1.000000

OBJECT 5: MIRROR 9
Physical Surface 5 (PLANE)
Box X 71.52 97.49 Y 78.44 104.4 Z 985.5 986.7
width= 25.973 width= 25.962 width= 1.2058
Interface Reflectivity 1.000000

OBJECT 6: MIRROR 10
Physical Surface 6 (BICONIC)
Box X 111.9 178.1 Y 62.40 129.2 Z 1087. 1112.
width= 66.132 width= 66.773 width= 24.575
Interface Reflectivity 1.000000

OBJECT 7: MIRROR 12
Physical Surface 7 (PLANE)
Box X 120.5 169.5 Y 62.02 113.2 Z 877.7 894.7
width= 49.024 width= 51.152 width= 16.977
Interface Reflectivity 1.000000

OBJECT 8: MIRROR 14
Physical Surface 8 (BICONIC)
Box X 228.2 341.7 Y 38.38 152.7 Z 1075. 1112.
width= 113.54 width= 114.35 width= 37.020
Interface Reflectivity 1.000000

OBJECT 9: MIRROR 15
Physical Surface 9 (PLANE)
Box X 275.7 353.3 Y 49.56 128.7 Z 916.5 936.1
width= 77.515 width= 79.142 width= 19.593
Interface Reflectivity 1.000000

OBJECT 10: IMAGE 16
Physical Surface 10 (PLANE)
Box X 375.3 475.1 Y 35.68 155.2 Z 1055. 1126.
width= 99.810 width= 119.49 width= 71.113
Transmission 1.000000 Media 0 0

OBJECT 11: IDEALENS
Physical Surface 11 (IDEAL)
Box X -2040. 2040. Y -2040. 2040. Z -3040. -2960.
width= 4080.0 width= 4080.0 width= 80.000
Transmission 1.000000 Media 0 0

```
OBJECT   12: SKY
Physical Surface   12 (OPTICAL )
    Box X -.3927E+5  .3927E+5 Y -.3927E+5  .3927E+5 Z -.3003E+7 -.3003E+7
      width= 78540.       width= 78540.       width= 78.500

OBJECT   13: COLDS
Physical Surface   13 (OPTICAL )
    Box X  178.4    236.8   Y  57.62    125.8   Z  965.0    1001.
      width= 58.394       width= 68.192       width= 35.744
      Transmission 1.000000 Media  0  0

OBJECT   14: FIELDS
Physical Surface   14 (OPTICAL )
    Box X  117.5    172.6   Y  64.91    120.1   Z  1016.    1018.
      width= 55.155       width= 55.155       width= 1.3636
      Transmission 1.000000 Media  0  0

OBJECT   15: WINS
Physical Surface   15 (OPTICAL )
    Box X  41.74    84.08   Y  74.78    122.1   Z  1012.    1040.
      width= 42.341       width= 47.344       width= 28.236
      Transmission 1.000000 Media  0  0
```

APART model.

TBD.